Journal of Alloys and Compounds 509 (2011) 10195–10202

Contents lists available at ScienceDirect

Journal of Alloys and Compounds

journal homepage: www.elsevier.com/locate/jallcom

Microwave dielectric properties of $(Zn_{1-x}Mg_x)TiO_3$ (ZMT) ceramics for dielectric resonator antenna application

Ravi Kumar Gangwar[a,*], S.P. Singh[a], Meenakshi Choudhary[b], Nitish Kumar Singh[b], Devendra Kumar[b], G. Lakshmi Narayana Rao[c], K.C. James Raju[c]

[a] Department of Electronics Engineering, Institute of Technology, Banaras Hindu University, Varanasi 221005, India
[b] Department of Ceramic Engineering, Institute of Technology, Banaras Hindu University, Varanasi 221005, India
[c] School of Physics, University of Hyderabad, Hyderabad 500046, India

ARTICLE INFO

Article history:
Received 18 January 2011
Received in revised form 12 June 2011
Accepted 5 August 2011
Available online 30 August 2011

Keywords:
ZMT ceramic material
DRA
Permittivity
Radiation pattern

ABSTRACT

Present investigation provides experimental studies on cylindrical dielectric resonator antennas (CDRAs) fabricated from $(Zn_{1-x}Mg_x)TiO_3$ (ZMT) ceramic material with different substitution of Mg in place of Zn ($x = 0.1$, 0.2, 0.3, 0.4 and 0.5) along with measurement of material permittivity in C-band of microwave frequencies. The dielectric properties of the ZMT ceramic materials with different x values ($x = 0.1$–0.5) have been measured at microwave frequencies using Hakki–Coleman method modified by Courtney. The value of dielectric constant and loss tangent decreases with the increase in Mg content. The dielectric constant is minimum for $x = 0.3$ and loss tangent is minimum for $x = 0.5$. The variations of return loss and input impedance versus frequency and radiation patterns of CDRAs at their respective resonant frequencies are studied experimentally. The measured results for resonant frequency and return loss bandwidth of the CDRAs are also compared with theoretical ones. The measured resonant frequencies of all the four CDRAs are nearly in agreement with respective theoretical values and the values of input resistance at respective resonant frequencies of the CDRAs match well with the coaxial feed impedance of 50 Ω. The designed CDRAs have broad beam, low side lobe and cross-polarized lobe levels.

1. Introduction

With the rapid development of global microwave communication in recent years, the demand for high-quality microwave devices has increased. Dielectric resonators (DRs) have been extensively used in microwave circuits, such as oscillators, filters and cavity resonators. In present decade, the antennas in microwave and millimeter wave band employing these types of resonators have been extensively studied [1–4]. These antennas have several advantages such as small size, low profile, high radiation efficiency, large bandwidth, flexible feed arrangement, wide range of material dielectric constants, ease of excitation, easily controlled characteristics and ease of integration with other active or passive microwave integrated circuit (MIC) components [5–9]. DRAs are available in various basic classical shapes such as rectangular, cylindrical, spherical and hemispherical geometries. Two dielectric properties of materials must be considered for DRA use. The first property is dielectric constant and the second one is quality factor. The size of DRA is inversely proportional to dielectric constant of material and losses in the DRA to quality factor of material.

Several dielectric materials have been developed for DRA applications. Zinc containing ceramics such as $(Zn,Mg)TiO_3$ are good aspirants for microwave dielectric devices owing to their high quality factor and relatively low loss. Recently, many investigators have focused attention on the substitution of the Zn site with Mg to form solid solutions and improve the dielectric properties of microwave materials [10–12]. The addition of V_2O_5 significantly improved the densification of $(Zn,Mg)TiO_3$ and the addition of glass additives in $(Zn_{1-x}Mg_x)TiO_3$ (ZMT) ceramics lowered the sintering temperature and improved the microwave dielectric properties [13,14]. Additionally, the increased amount of magnesium raised both the sintering temperature and the decomposition temperature of $(Zn,Mg)TiO_3$. Dielectric properties of microwave $(Zn,Mg)TiO_3$ ceramics depend on the densification and phase structure. As the amount of magnesium content is increased, relative permittivity of $(Zn,Mg)TiO_3$ dielectrics decreased which is accompanied with increase in $Q \times f$ value.

In this paper, the synthesis and characterization of $(Zn_{1-x}Mg_x)TiO_3$ (ZMT) ceramic materials with different x values ($x = 0.1$, 0.2, 0.3 and 0.4) and radiation characteristics of cylindrical dielectric resonator antennas (CDRAs) fabricated using

* Corresponding author. Tel.: +91 542 6701258; fax: +91 542 2366758.
E-mail address: ravi.gangwar.ece07@itbhu.ac.in (R.K. Gangwar).

0925-8388/$ – see front matter © 2011 Elsevier B.V. All rights reserved.
doi:10.1016/j.jallcom.2011.08.028

these materials are reported at microwave frequencies. The dielectric properties of ZMT ceramic materials synthesized with different x values ($x = 0.1$, 0.2, 0.3, 0.4 and 0.5) are characterized. The radiation characteristics of the fabricated CDRAs at their respective resonant frequencies are investigated experimentally. Measured results for resonant frequency and bandwidth are compared with theoretical ones.

2. Materials, synthesis and characterization

The $(Zn_{1-x}Mg_x)TiO_3$ (ZMT) materials in powder form with x values varying from 0.1 to 0.5 using step interval of 0.1 were prepared using solid state ceramic route. ZnO [99.5%, S.D. Fine Chemical Ltd], MgO [96%, Thomas Baker (Chemicals) Pvt. Ltd] and TiO_2 [99.5%, Reidal (India) Chemicals] were used as starting materials. Stoichiometric amounts of all the compounds were taken and mixed thoroughly in an agate mortar with pestle for 2 h using acetone as mixing media. The mixed powders were then transferred into zirconia jar and ball milled with the help of zirconia grinding media for 4 h using acetone as mixing medium. The mixed powders were dried in air and calcined in an alumina crucible at 1200 °C using an electrical furnace. The calcined powders were ground and mixed uniformly with a few drops of 2 wt% solution of polyvinyl alcohol (PVA) acting as a binder. Binder mixed powders were then pressed into pellets under optimum load of 70 kN in cylindrical shape with radius-to-height ratio of 2:1 using a uniaxial hydraulic press. These pellets were sintered at 1300 °C for 4 h in air. For sintering, pellets were kept on alumina plate, heated slowly up to 500 °C and kept at this temperature for about 2 h to burn off the binder completely. Thereafter, the temperature was raised to required sintering temperature at a rate of 5 °C/min, soaked at this temperature for 4 h and then cooled to room temperature at a rate of 5 °C/min.

Density of the sintered pellets was measured using Archimedes Principle. The sintered pellets were ground and powder X-ray diffraction patterns were recorded using Seifert X-ray Diffractometer employing Cu-Kα_1 radiation using a Ni filter. Sintered pellets were polished using emery papers of grade 1/0, 2/0, 3/0, 4/0 and 5/0 (Sia, Switzerland) successively followed by polishing on a velvet cloth with diamond paste of grade 1/4-OS-475 (HIFIN). Then, they were etched chemically using a solution containing 10% of acetic acid. Chemically etched pellets were washed in distilled water and coated with gold by sputtering technique. The micrographs were recorded using ZEISS scanning electron microscope (FE-SEM, Model No. SUPRA-40, USA). Phases of solid solutions were confirmed by powder XRD. XRD patterns for solid solution of different compositions of system $(Zn_{1-x}Mg_x)TiO_3$ (ZMT) with $x = 0.1$–0.5 are shown in Fig. 1(a)–(e). Phases of different compounds were identified using standard JCPDS files of possible compounds which can be formed during reactions. Identified phases of different compounds are indexed in Fig. 1(a)–(e). This shows that all the compositions have $(Mg,Zn)TiO_3$, $(Mg,Zn)Ti_2O_5$ and TiO_2 phases. The proportions of different phases depend on composition. It is observed that increasing the content of Mg suppresses the phase of un-reacted TiO_2 and promotes the formation of $(Mg,Zn)Ti_2O_5$ phase. The experimental density of the sintered pellets determined using Archimedes principle is given in Table 1. It can be seen from Table 1 that the density of the sintered ZMT ceramic decreases with increase in Mg content. The decrease in density may be due to the precipitation of $MgTi_2O_5$. Fig. 2 shows the SEM of the compositions with x values varying from 0.1 to 0.5. From Fig. 2 it can be observed that all compositions have agglomerated nano grains with dense structure. It is also observed that size of the grains increases with increasing Mg content.

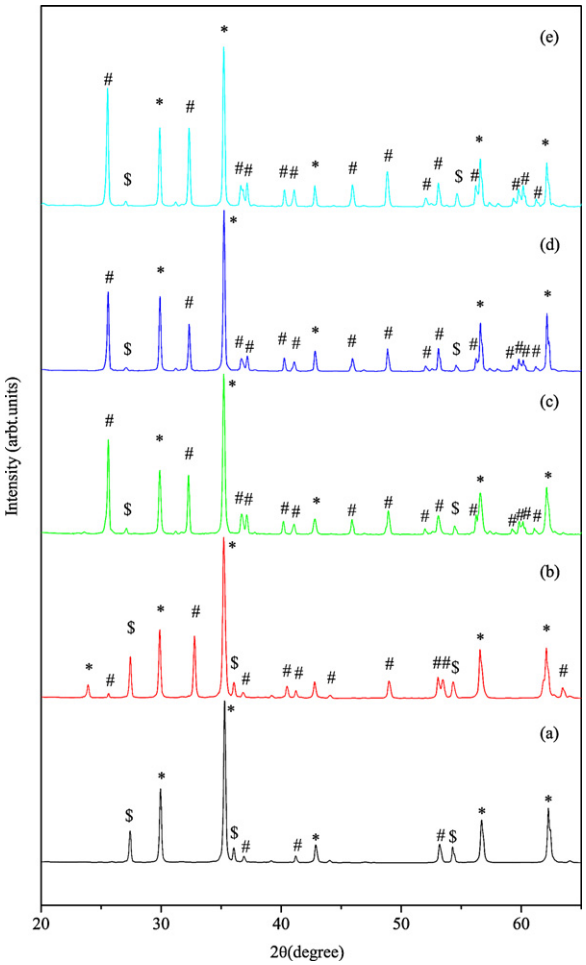

Fig. 1. X-ray diffraction patterns of $(Zn_{1-x}Mg_x)TiO_3$ with (a) $x = 0.1$, (b) $x = 0.2$, (c) $x = 0.3$, (d) $x = 0.4$ and (e) $x = 0.5$ (where $^*(Mg,Zn)TiO_3$, $^\#(Mg,Zn)Ti_2O_5$ and $^\$TiO_2$).

Table 1
Experimental density of ZMT ceramic materials.

Compositions with x	Density (gm/cm^3)
0.1	4.62615
0.2	4.23734
0.3	3.96533
0.4	3.93987
0.5	3.85424

3. Measurement of dielectric constant of ZMT ceramic material

Microwave dielectric properties of ZMT ceramic materials in the frequency range of 2–10 GHz were measured using an Agilent PNA series Vector Network Analyzer (Model No.: 8722ES). The values of dielectric constant (ε_r) and loss tangent ($\tan\delta$) are obtained using TE_{011} resonance mode of the end-shorted sample placed between two conducting plates, using the method of Hakki and Coleman [15] and modified by Courtney (Fig. 3(a)). The reflection method was used for measuring the Q-factor, in which the sample was placed at the center of a cylindrical resonant cavity having dimensions three times greater than the sample dimensions (Fig. 3(b)). The measurement was done using TE_{011} mode of the under coupled resonator and the correction for the coupling coefficient was applied [16]. The experimentally determined values of dielectric constant and loss tangent of the ceramic materials are given in Table 2.

From Table 2 it can be observed that the value of dielectric constant and loss tangent decreases with increase in Mg content. The dielectric constant is minimum for $x = 0.3$ and loss tangent is minimum for $x = 0.5$. This shows that increasing amount of Mg content improves the loss property of the ZMT material. The high value of dielectric constant as well as loss tangent of material for the compositions $x = 0.1$ and 0.2 may be due to the presence of more un-reacted TiO_2 and the lower value of rest of the compositions may be attributed to less amount of un-reacted TiO_2 and decreasing density. Variation in the value of dielectric constant of material for compositions with $x = 0.3$, 0.4 and 0.5 may be due to different proportion of phases $(Mg,Zn)TiO_3$ and $(Mg,Zn)Ti_2O_5$ present in these compositions. The decrease in the value of dielectric constant in the later compositions may be attributed to increase of grain size i.e. decrease in overall area of grain boundaries.

4. Antenna design

The configuration of CDRAs fabricated from $(Zn_{1-x}Mg_x)TiO_3$ (ZMT) ($x = 0.1$–0.4) ceramic materials sintered at 1300 °C is shown

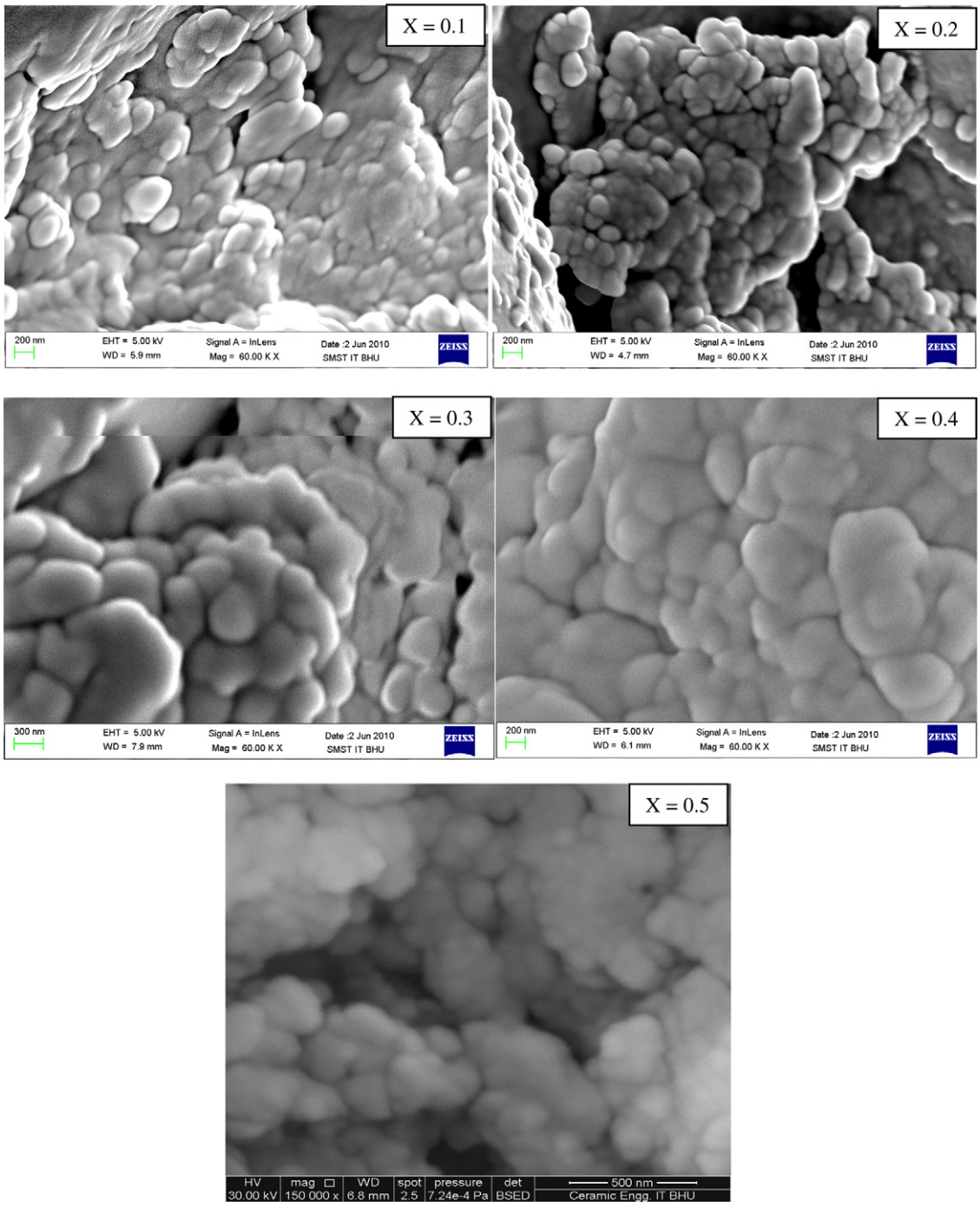

Fig. 2. SEM of ZMT ceramic materials with different *x*-values.

in Fig. 4. Each DRA is placed on a conducting ground plane (copper conductor of size 60 mm × 60 mm × 4 mm is used as ground plane). The DRAs fabricated from ZMT ceramic materials are excited by 50 Ω coaxial probes of same diameter (=1.3 mm) but different lengths which were optimized to provide minimum return loss at the corresponding resonant frequencies. In Fig. 4 the radius, height and dielectric constant of the DRA are denoted by a, h and ε_r. The probe is located on x-axis at $x = a$ and $\Phi = 0$.

Table 2
Dielectric properties of ZMT ceramic material.

Material	Diameter (mm)	Height (mm)	Resonant frequency (GHz)	Dielectric constant	tan δ	Q
ZMT-0.1	14.81	6.83	4.4675	26.221	1.25E−03	7.98E+02
ZMT-0.2	14.66	6.28	5.3025	19.452	4.56E−04	2.19E+03
ZMT-0.3	14.67	7.85	5.74	15.698	4.54E−04	2.20E+03
ZMT-0.4	14.27	9.01	5.3361	17.799	8.07E−04	1.24E+03
ZMT-0.5	13.87	8.18	5.535	17.736	4.26E−04	2.35E+03

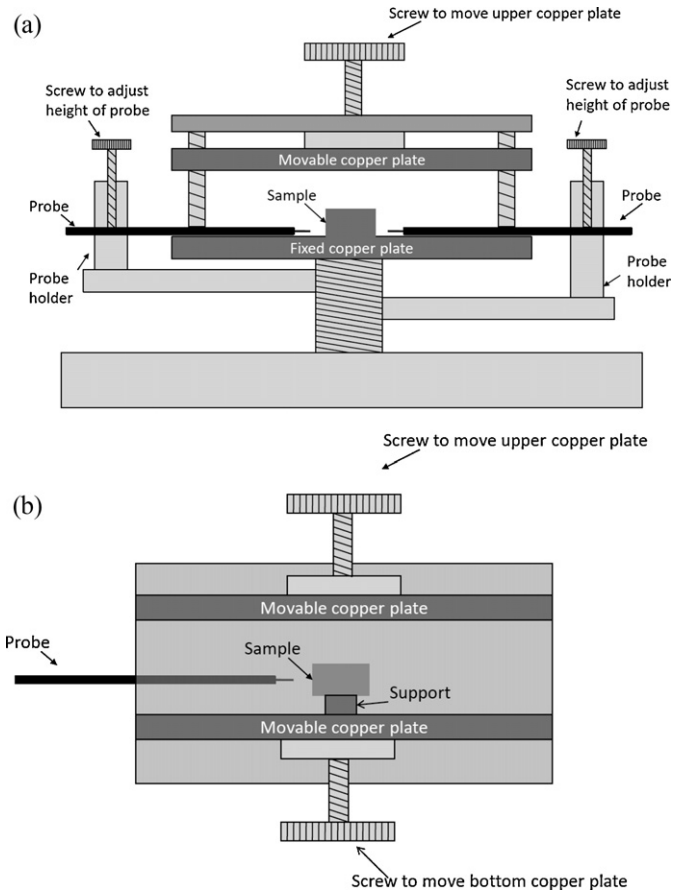

Fig. 3. Setup for (a) ε_r measurement and (b) Q-factor measurement.

The resonant frequency of single segment CDRA excited in $HEM_{11\delta}$ mode can be written as [5,17]

$$f = \frac{6.324c}{2\pi a\sqrt{2+\varepsilon_r}}\left\{0.27 + 0.36\frac{a}{2h} + 0.02\left(\frac{a}{2h}\right)^2\right\} \quad (1)$$

where $a = D/2$, D is the diameter of CDRA, h is the height of the CDRA above ground plane, c is the velocity of microwave in free space ($=3\times10^8$ m/s), and ε_r is the relative permittivity of CDRA material.

Eq. (1) has been obtained through curve fitting and numerical simulations based on the method of moments [5,18].

Radiation Q-factor of isolated CDRA can be written as [5,17]

$$Q = 0.01007(\varepsilon_r)^{1.3}\left(\frac{a}{h}\right)[1 + 100e^{-[2.05(a/2h)-(1/80(a/h)^2)]}] \quad (2)$$

The percentage bandwidth of isolated CDRA is given by [5,17].

$$\%BW = \frac{S-1}{Q\sqrt{S}} \times 100 \quad (3)$$

where S is the VSWR of isolated CDRA.

The resonant frequency, Q-factor and bandwidth of the four DRAs are computed using Eqs. (1)–(3), assuming that ε_r value remains constant in 3.6–5.8 GHz frequency range and using measured ε_r values in computation of the parameters.

5. Experimental results and discussion

5.1. Return loss versus frequency characteristics

Measurement of return loss of CDRAs with coaxial probe feed was carried out over 3–5 GHz frequency range using Agilent PNA series Vector Network Analyzer (Model No.: E8364 B). The measured variations of return loss with frequency for the CDRAs are shown in Fig. 5. From Fig. 5 the resonant frequency and percentage bandwidth of the proposed CDRAs are extracted and the results are shown in Table 3.

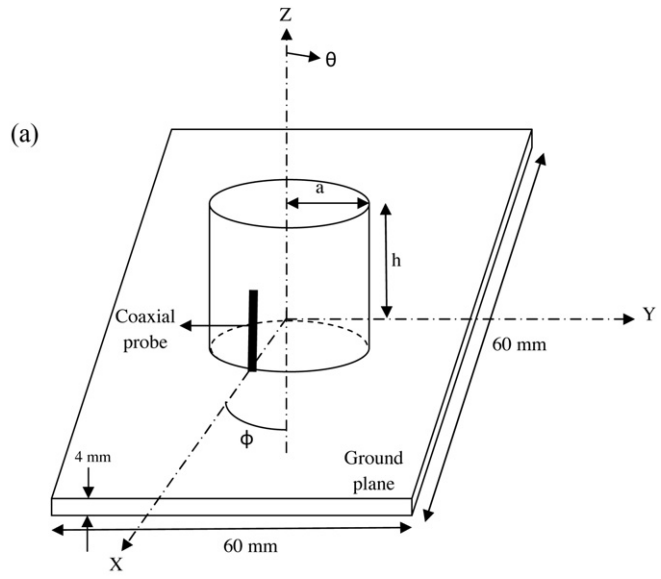

Fig. 4. Antenna geometry (a) layout and (b) fabricated structure.

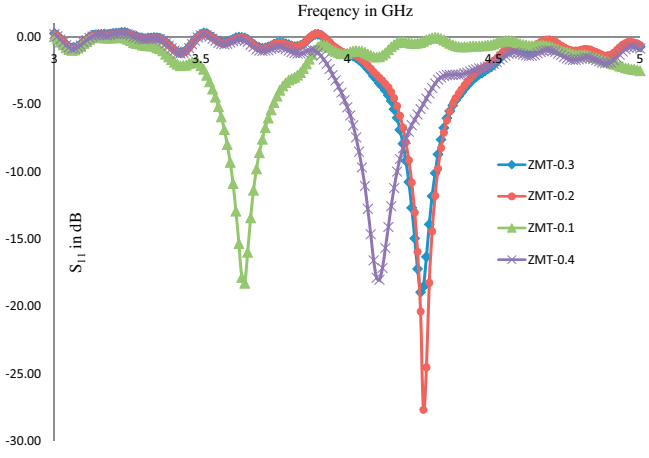

Fig. 5. Variation of return loss with frequency.

Table 3
Resonant frequency and return loss performance of ZMT CDRAs.

Sample	ε_r	D (mm)	h (mm)	Resonant frequency in GHz		Return loss bandwidth in %	
				Theoretical	Experimental	Theoretical	Experimental
ZMT-0.1	26.221	14.81	6.83	3.61	3.65	2.65	2.47
ZMT-0.2	19.452	14.66	6.28	4.32	4.26	3.93	2.01
ZMT-0.3	15.698	14.67	7.85	4.32	4.26	5.20	2.11
ZMT-0.4	17.799	14.27	9.01	4.17	4.11	4.50	2.67

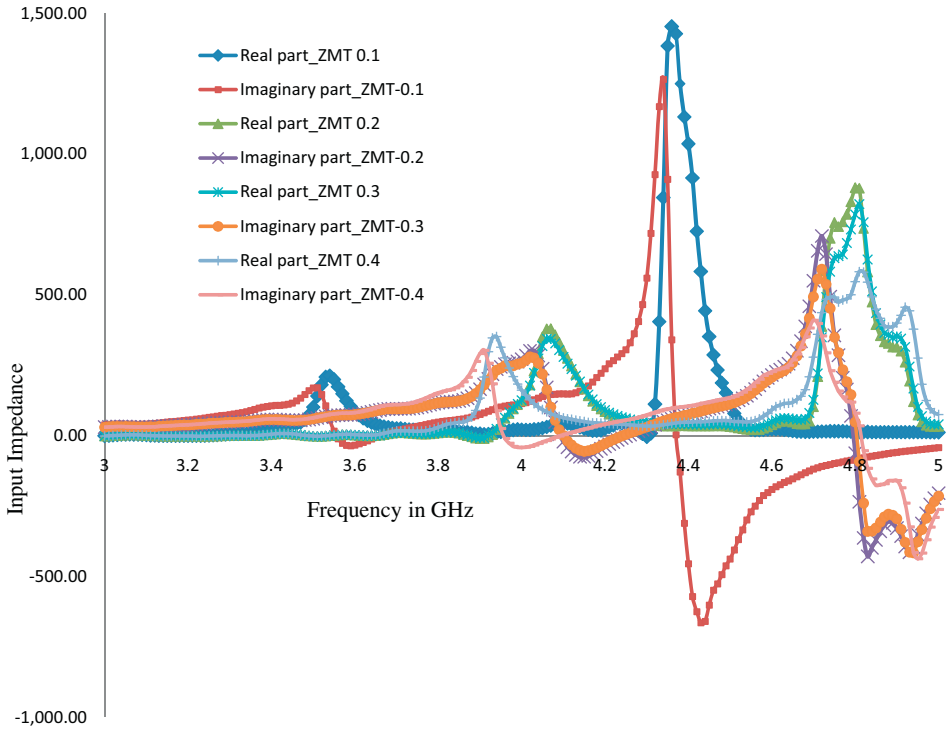

Fig. 6. Variation of input impedance with frequency.

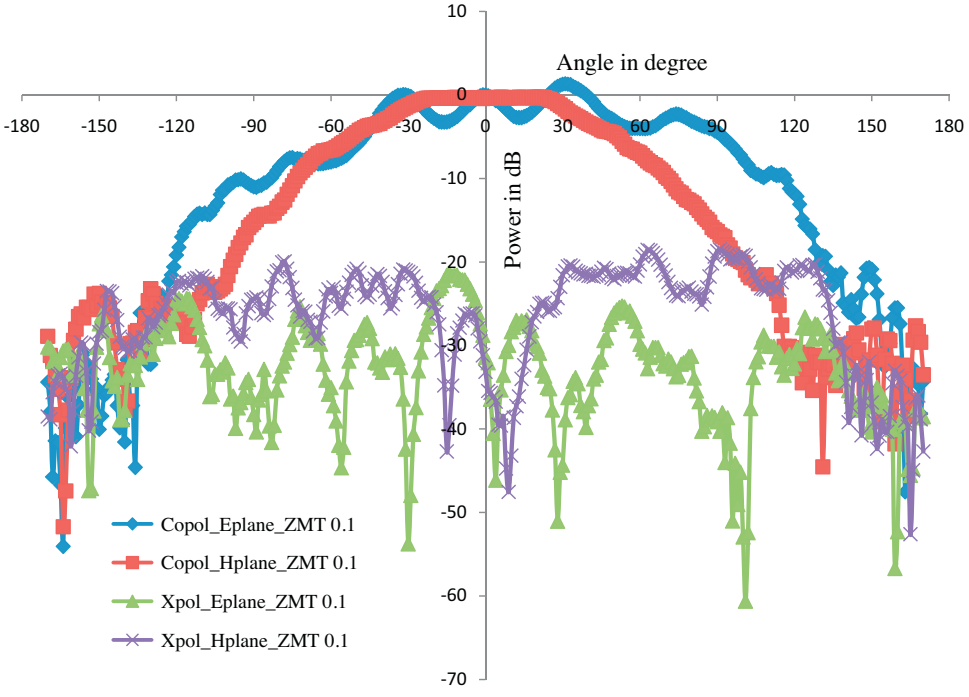

Fig. 7. Radiation pattern of CDRA fabricated from ZMT-0.1 material.

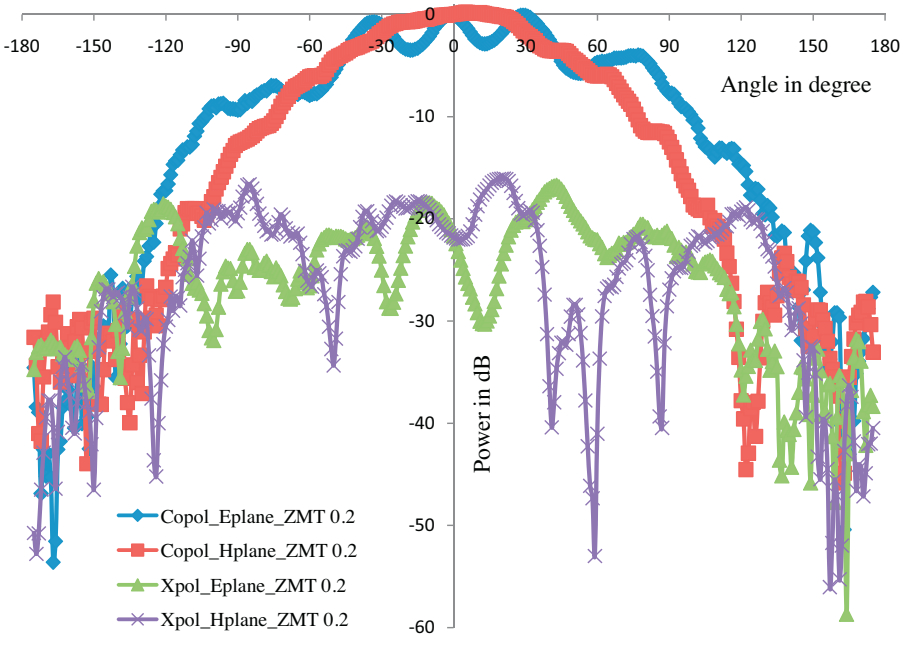

Fig. 8. Radiation pattern of CDRA fabricated from ZMT-0.2 material.

From Fig. 5 and Table 3 it can be observed that the measured resonant frequency of all the four CDRAs is nearly in agreement with respective theoretical values. The measured bandwidth of the antennas is lower than the corresponding theoretical ones. The deviation in the results may be due to probe coupling, fabrication tolerances, effect of finite ground plane not considered in theoretical computation, and the effect of adhesive used to bind the DRAs to ground plane during fabrication of antennas.

5.2. Input impedance versus frequency characteristics

Measurement of input impedance of the fabricated CDRAs at different frequencies over 3–5 GHz range with coaxial probe feed was carried out using Agilent PNA series Vector Network Analyzer (Model No.: E8364 B). The measured variations of input impedance with frequency are shown in Fig. 6. It is worth mentioning that the values of input resistance at respective resonant frequencies of the CDRAs match well with 50 Ω coaxial feed.

From Fig. 6 it can also be seen that in each case the input reactance has an upward shift due to the inductive loading of the probe and consequently the frequency at which the input resistance is maximum does not coincide with the zero-reactance frequency.

5.3. Far field performance

The co-polar and cross-polar radiation patterns of the fabricated CDRAs for $\Phi = 0^\circ$ (x–z plane) and $\Phi = 90^\circ$ (y–z plane) were measured in anechoic chamber at their respective resonant frequencies.

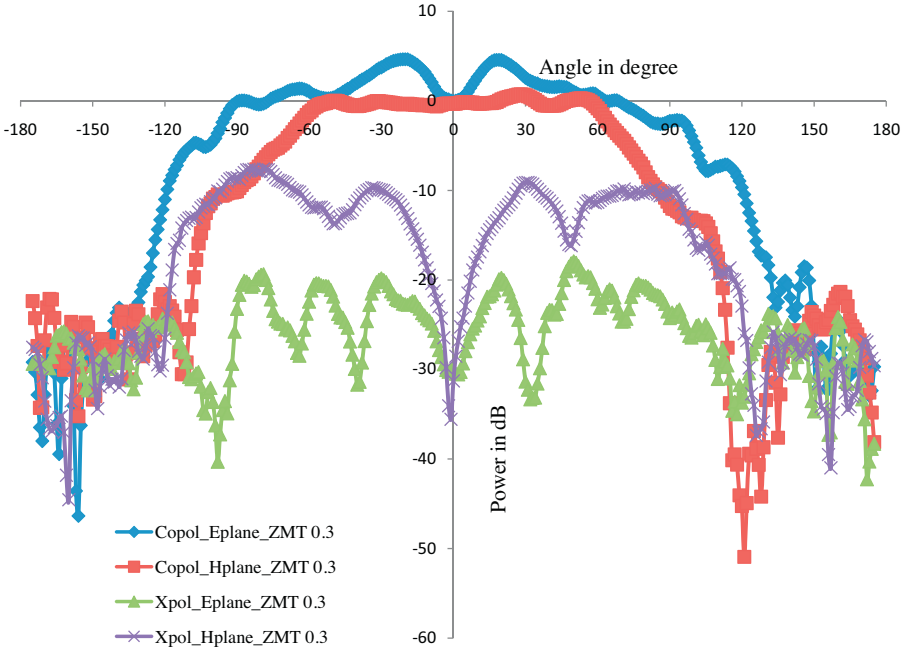

Fig. 9. Radiation pattern of CDRA fabricated from ZMT-0.3 material.

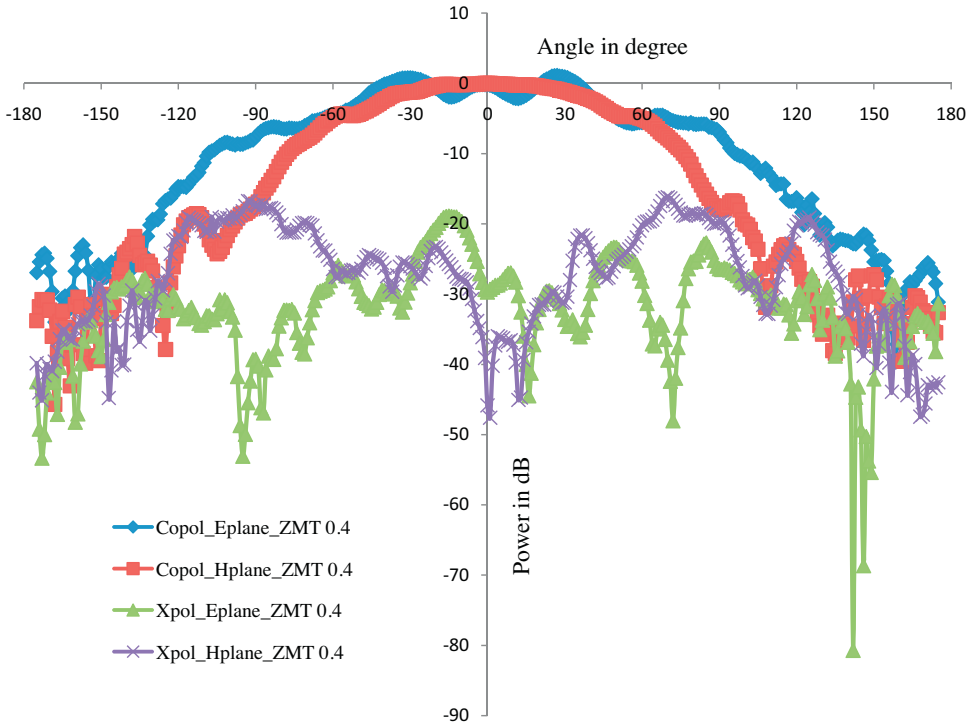

Fig. 10. Radiation pattern of CDRA fabricated from ZMT-0.4 material.

Table 4
Far field performance of ZMT CDRAs.

Far field parameters		ZMT-0.1	ZMT-0.2	ZMT-0.3	ZMT-0.4
Gain in dB		4.29	6.98	6.40	6.04
HPBW	E-plane	63°	56°	195°	96°
	H-plane	77°	75°	133°	87°
Ripple	E-plane	1.338 dB	−0.067 dB	4.642 dB	1.072 dB
Cross-polarization level	E-plane	−21.351 dB	−16.709 dB	−17.97 dB	−18.89 dB
	H-plane	−20.395 dB	−16.077 dB	−9.11 dB	−16.211 dB

The experimental setup is not shown here for brevity. The far field patterns (E- and H-planes) of the CDRAs are shown in Figs. 7–10, respectively. The far field parameters of CDRAs are extracted from Figs. 7–10, and the results are given in Table 4.

From Figs. 7–10 it can be observed that the E-plane patterns are somewhat asymmetrical. This may be due to the finite size of coaxial probe which causes spurious radiation. The spurious radiation from the coaxial probe as well as the finite size of ground plane result in ripples in the E-plane patterns of up to 4 dB, whereas the H-plane patterns do not reveal ripples and are close to the ideal pattern of the short magnetic dipole model. These figures also show that these antennas provide broad beam, low side lobe and cross-polarized lobe levels.

From Table 4 it can be seen that the gain of the CDRA fabricated from ZMT-0.1 is lower than others. This is due to greater loss tangent of the material of composition with $x = 0.1$ as compared with others compositions. It can be also observed that HPBW and ripple of the CDRA (ZMT-0.2) is the lowest.

The CDRA fabricated from material of composition with $x = 0.2$ can be used as an element in a phased array for radar and communication application because of its relatively high gain and least ripple amplitude. The antenna fabricated from material composition with $x = 0.3$ can find application in wireless communication including WLAN and WiMAX due to its broadest beam and reasonable gain. Based on requirement antenna can be fabricated from the material having one of the compositions studied.

6. Conclusion

In this paper design, fabrication and testing of low profile CDRAs fabricated from ZMT ceramic materials with x-value varying from 0.1 to 0.4 sintered at 1300 °C along with measurement of permittivity of materials with x-values varying from 0.1 to 0.5 in C-band of microwave frequencies are presented. The CDRAs designed and fabricated from low loss high dielectric constant ceramic composites provided broad beam, low side lobe and cross-polarized lobe levels. The measurements have confirmed the use of high dielectric constant and low loss ceramic materials for designing CDRAs. The experimental results presented here may be utilized to design and fabricate an appropriate DRA for potential applications in wireless communication and radar fields.

References

[1] Z. Peng, H. Wang, X. Yao, Ceramics International 30 (2004) 1211–1214.
[2] Y.-C. Huang, M.-C. Wu, T.-H. Chang, J.-F. Kiang, W.-F. Su, Journal of the European Ceramic Society 27 (2007) 2841–2844.
[3] Y.-C. Chen, S.-M. Tsao, C.-S. Lin, S.-C. Wang, Y.-H. Chien, Journal of Alloys and Compounds 471 (2009) 347–351.
[4] I.S. Ghosh, A. Hilgers, T. Schlenker, R. Porath, Journal of the European Ceramic Society 21 (2001) 2621–2628.
[5] R.K. Mongia, P. Bhartia, International Journal of Microwave and Millimeter Wave Computer-Aided Engineering 4 (1994) 230–247.
[6] A. Ittipiboon, R.K. Mongia, IEEE Transactions on Antennas and Propagation 45 (1997) 1348–1356.

[7] P. Rezaei, M. Hakkak, K. Forooaghi, Progress in Electromagnetics Research 66 (2006) 111–124.
[8] D. Kajfez, A.A. Kishk, Proceedings VITEL 2002, International Symposium on Telecommunications, Next Generation Networks and Beyond, Portoroz, Slovenia, May 13–14, 2002.
[9] M. Saed, R. Yadla, Progress in Electromagnetics Research 56 (2006) 151–162.
[10] Y.S. Chang, Y.-H. Chang, I.G. Chen, G.J. Chen, Solid State Communications 128 (2003) 203–208.
[11] H.T. Kim, Y.H. Kim, Journal of the Korean Physical Society 32 (1998) S346–S348.
[12] Y.C. Zhang, J. Wang, Z.X. Yue, Z.L. Gui, L.T. Li, Ceramics International 30 (2004) 87–91.
[13] M.-L. Hsieh, L.-S. Chen, H.-C. Hsu, S. Wang, M.-P. Houng, S.-L. Fu, Materials Research Bulletin 43 (2008) 3122–3129.
[14] W.R. Wang, S.F. Wang, Y.M. Lin, Ceramics International 31 (2005) 905–909.
[15] B.W. Hakki, P.D. Coleman, IEEE Transactions on Microwave Theory and Techniques 8 (1960) 402–410.
[16] D. Kajfez, E.J. Hwan, IEEE Transactions on Microwave Theory and Techniques 32 (1984) 666–670.
[17] A.A. Kishk, A.W. Glisson, G.P. Junker, Antenna Application Symposium (1999) 45–68.
[18] A.A. Kishk, A.W. Glisson, D. Kajfez, IEEE Antennas and Propogation Society International Symposium Digest (1993) 408–411.